

Role of Eckhaus instability and pattern cracking in ultraslow dynamics of Kerr combsDamià Gomila ^{1,*}, Pedro Parra-Rivas ², Pere Colet,¹ Aurélien Coillet,^{3,4} Guoping Lin,^{3,5} Thomas Daugey,³ Souleymane Diallo,³ Jean-Marc Merolla,³ and Yanne K. Chembo^{3,6,†}¹*Instituto de Física Interdisciplinar y Sistemas Complejos, IFISC (CSIC-UIB), Campus Universitat de les Illes Balears, E-07122 Palma de Mallorca, Spain*²*Department of Information Engineering, Electronics and Telecommunications, Sapienza University of Rome, Via Eudossiana 18, 00184 Rome, Italy*³*FEMTO-ST Institute, Université Bourgogne Franche-Comté, CNRS, 15B Avenue des Montboucons, 25030 Besançon cedex, France*⁴*Laboratoire Interdisciplinaire Carnot de Bourgogne, Université Bourgogne-Franche-Comté, CNRS, 9 Avenue A. Savary, 21078 Dijon, France*⁵*MOE Key Laboratory of Fundamental Quantities Measurement, School of Physics, Huazhong University of Science and Technology, Wuhan 430074, China*⁶*Department of Electrical and Computer Engineering, Institute for Research in Electronics and Applied Physics (IREAP), University of Maryland, 8279 Paint Branch Drive, College Park Maryland 20742, USA* (Received 7 September 2022; accepted 2 November 2022; published 28 November 2022)

The Eckhaus instability is a secondary instability of nonlinear spatiotemporal patterns in which high-wave-number periodic solutions become unstable against small-wave-number perturbations. Here we show that this instability can take place in Kerr combs corresponding to subcritical Turing patterns upon changes in the laser detuning. The development of the Eckhaus instability leads to the cracking of patterns and a long-lived transient where the peaks of the pattern rearrange in space due to spatial interactions. In the spectral domain, this results in a metastable Kerr comb dynamics with timescales that can be larger than 1 min. This time is, at least, seven orders of magnitude larger than the intracavity photon lifetime and is in sharp contrast with all the transient behaviors reported so far in cavity nonlinear optics that are typically only a few photon lifetimes long (i.e., in the picosecond to the microsecond range). This phenomenology, studied theoretically in the Lugiato-Lefever model and the observed dynamics is compatible with experimental observations in Kerr combs generated in ultra-high- Q whispering-gallery mode resonators.

DOI: [10.1103/PhysRevA.106.053518](https://doi.org/10.1103/PhysRevA.106.053518)

Kerr optical frequency combs are obtained through pumping a high- Q whispering-gallery mode (WGM) cavity with a resonant laser [1]. In the past decade, the experimental and theoretical studies of these combs have permitted major advances in photonics (see review articles [2–5]). From the applications standpoint, Kerr combs have been developed for time-frequency metrology, ultrastable microwave generation, spectroscopy, and optical communications, just to name a few. From the fundamental perspective, Kerr combs have provided an ideal platform to investigate light-matter interactions in confined media. It has been shown that a wide variety of dissipative structures could be excited in the WGM resonators, being either stationary (azimuthal stripe or roll patterns, cavity solitons, platicons) or nonstationary (breather solitons, spatiotemporal chaos, and rogue waves). The primary bifurcations leading to these various patterns have also been the focus of a detailed analysis in the literature [6–13]. However, only a limited attention has been also devoted to secondary

bifurcations, which lead to the destabilization of the stationary patterns [13–16].

In this paper we study theoretically the Eckhaus (EC) instability of stripe patterns in one dimension, which emerges when a pattern loses its stability against small-wave-number perturbations (see Refs. [17–19]). The Eckhaus instability has long been studied in fluid mechanics [20,21], liquid crystals [22], nonlinear optics [13,14,23–25], or systems with delayed feedback [26]. Experimental observations are, however, much more limited since large aspect-ratio patterns are required, whereas being difficult to attain in most systems. The Eckhaus instability can also be induced by spatial inhomogeneities [24,27], an effect that has been observed experimentally in a liquid-crystal layer with optical feedback [23]. Other secondary instabilities and parametric perturbations may also hinder Eckhaus instabilities [21,22]. Counterintuitively, despite their relatively small size, WGM resonators can output large aspect-ratio stripe patterns with tens or even hundreds of peaks [28], making the system more susceptible to develop small-wave-number (or long-wavelength) instabilities.

The theoretical analysis of the Eckhaus instability starts with the Lugiato-Lefever equation (LLE) [29], which is an

*damia@ifisc.uib-csic.es

†ykchembo@umd.edu

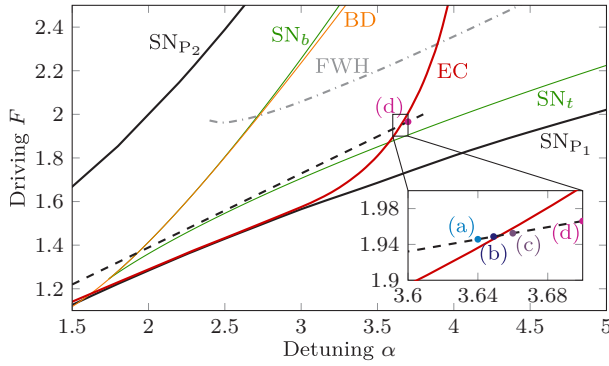


FIG. 1. Bifurcation lines of the homogeneous solutions and the stripe pattern with $L = 55$ in the parameter space (α, F) . The homogeneous steady state (HSS) is stable below the modulational instability (MI) (yellow line for $\alpha < 2$) and below the SN_b line for $\alpha > 2$. The pattern is stable above the EC line and below the SN_{P_2} or the finite-wavelength Hopf (FWH) line, whichever comes first. The dashed line shows the ramp of parameters applied to the pattern, starting from $(\alpha, F) = (1, 1.05)$ to $(3.8, 2)$ beyond the Eckhaus instability.

accurate model to analyze the laser field dynamics in Kerr-nonlinear WGM resonators [30–32]. The slowly varying complex amplitude of the normalized intracavity field $\psi(\theta, \tau)$ obeys the equation,

$$\frac{\partial \psi}{\partial \tau} = -(1 + i\alpha)\psi - i\frac{\beta}{2}\frac{\partial^2 \psi}{\partial \theta^2} + i|\psi|^2\psi + F, \quad (1)$$

where $\theta \in [-\pi, \pi]$ is the azimuthal coordinate along the ring of the resonator, and $\tau = t/2\tau_{\text{ph}}$ is the time scaled to the photon lifetime. The normalized parameters of this equation are the continuous-wave pump field F , the frequency detuning between laser and pumped resonance frequencies α , and the group-velocity dispersion β [31].

Equation (1) has homogeneous steady-states ψ_s implicitly given by $\rho_s[1 + (\rho_s - \alpha)^2] = F^2$ with $\rho_s = |\psi_s|^2$. The solution is trivalued for $\alpha > \sqrt{3}$. The line SN_b (respectively, SN_t) in Fig. 1 corresponds to the saddle-node bifurcation where lower (respectively, upper) and middle branches meet so that SN_b and SN_t unfold from the cusp at $\alpha = \sqrt{3}$ [6,7]. For $\alpha < \sqrt{3}$ the solution is monovalued. In what follows we refer to the lower homogeneous steady state as HSS.

In the anomalous regime ($\beta < 0$) and for $\alpha < 2$, $\rho_s = 1$ is the MI threshold above which the HSS is unstable to perturbations with wave-number L in the neighborhood of $L_u = \sqrt{(2/\beta)(\alpha - 2\rho_s)}$ (see Fig. 1). Stripe patterns with different wave numbers can emerge although typically the one with wave-number L_u dominates since it has the largest growth ratio. The wave-number L of the pattern determines the integer number of azimuthal stripes, or rolls, fitting the inner periphery of the disk. In the spectral domain, these stripe patterns correspond to the so-called *primary combs* where the teeth have a $L \times$ free-spectralrange (FSR) separation [6,7,33]. Patterns are supercritical for $\alpha < 41/30$ and subcritical for $\alpha > 41/30$. Regarding stripe patterns with other possible wave numbers, it turns out that only those with wave numbers close to L_u are stable, forming what is known as a *Busse balloon* [18,19] whereas patterns with wave numbers outside

the balloon are unstable. Moreover, in the subcritical regime, cavity solitons or localized states (LSs) coexist with the periodic patterns and the HSS. For $\alpha > 2$ the critical wave number is zero and the threshold $\rho_s = 1$ is a Belyakov-Devaney (BD) transition of the HSS [7,13] (see Fig. 1).

To study the secondary bifurcations that destabilize a stripe pattern of wave-number L we perform a linear stability analysis. The stationary but θ -dependent pattern can be expanded in Fourier series as

$$\psi_p(\theta) = \sum_{n=-N}^{N-1} \psi_n e^{inL\theta}, \quad (2)$$

with L being the integer wave number (or order) of the pattern and ψ_n being the complex amplitudes of the Fourier modes. We take $N = 32$, and the amplitudes can be calculated numerically by solving the stationary problem using a Newton-Raphson algorithm. Linearizing Eq. (1) about the stationary pattern $\psi_p(\theta)$ yields the perturbation equation,

$$\begin{aligned} \partial_\tau \delta\psi &= -(1 + i\alpha)\delta\psi - i(\beta/2)\partial_\theta^2 \delta\psi \\ &+ 2i|\psi_p|^2 \delta\psi + i\psi_p^2 \delta\psi^*. \end{aligned} \quad (3)$$

Due to the periodicity of the system, the solution of Eq. (3) can be written as the superposition of Bloch waves,

$$\delta\psi(\theta, \tau) = e^{iq\theta} \delta a(\theta, \tau, q) + e^{-iq\theta} \delta a(\theta, \tau, -q), \quad (4)$$

where δa has the same periodicity of the pattern $\psi_p(\theta)$ and can be written as

$$\delta a(\theta, \tau, q) = \sum_{n=-N}^{N-1} \delta a_n(\tau, q) e^{inL\theta}, \quad (5)$$

with q being an integer. Using Eq. (3), a set of linear equations for the Fourier modes $\delta a_n(\theta, q)$ can be derived [34], and in compact form they read as

$$\partial_\tau \Upsilon(\tau, q) = \mathbf{M}(\{\psi_n\}, q) \Upsilon(\tau, q), \quad (6)$$

where $\Upsilon(\tau, q) \equiv [\delta a_{-N}(\tau, q), \dots, \delta a_{N-1}(\tau, q), \delta a_{-N}^*(\tau, -q), \dots, \delta a_{N-1}^*(\tau, -q)]$. The stability analysis of $\psi_p(\theta)$ reduces to find the $2N$ eigenvalues $\{\lambda_n(q)\}$ of the matrix $\mathbf{M}(\{\psi_n\}, q)$, and its corresponding eigenvectors for each value of q . The eigenvalues for a given integer q determine the stability of the pattern against perturbations containing any set of wave-numbers $nL \pm q$. For this analysis it is sufficient to consider only the q values inside the first Brillouin zone $[0, L/2]$. We recall that the zero eigenvalue for $q = 0$ corresponds to the Goldstone mode associated with the translational invariance, and modes with $q \gtrsim 0$ form the branch of soft modes.

Figure 1 shows the bifurcation lines of the stripe pattern created spontaneously with the most unstable wave-number L_u for $\alpha = 1$ and $F = 1.05$ ($\rho_s = 1.095$). For the value of $\beta = -8 \times 10^{-4}$ considered here, we have $L_u = 55$. As the detuning is increased, the pattern becomes subcritical for $\alpha \simeq 41/30$, and above this value it exists between the saddle-node lines SN_{P_1} and SN_{P_2} , although unstable below the EC line. Above a certain value of the detuning and the pump, we observe a FWH instability (dot dashed) leading to oscillatory patterns [13,34]. We will not consider this regime here since we focus on the Eckhaus instability. Note that pattern and HSS

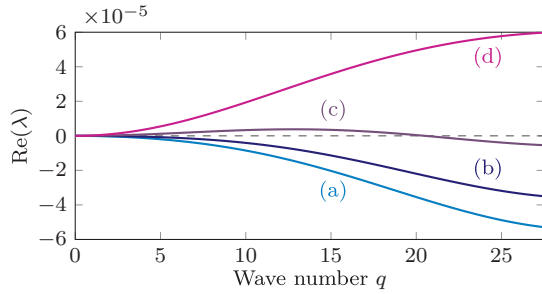


FIG. 2. Real part of the eigenvalues of the pattern with $L = 55$ for the branch of soft modes obtained from Eq. (6). Lines (a)–(d) correspond to the parameter values indicated by dots in Fig. 1. The curvature of the branch progressively changes from negative to positive signaling the Eckhaus instability.

are stable and coexist in the parameter region limited by MI, SN_b , FWH, and EC lines.

Figure 2 shows the real part of the eigenvalues of the pattern as a function of the wave-number q for the branch of soft modes [34]. The parameters correspond to those indicated by the dots in the inset of Fig. 1, crossing the Eckhaus instability. The change in convexity of the branch at $q = 0$ is what precisely signals the Eckhaus instability. After the instability, the pattern becomes unstable to small-wave-number perturbations. Well beyond the instability, the wave number of the mode maximum growth rate tends to the edge of the Brillouin zone $q = L/2$.

After encountering an Eckhaus instability a pattern with a wave number which is too large to be stable loses cells in such a way that the new wave number lies in the stability balloon [14]. For supercritical patterns this happens at a relatively fast timescale. For subcritical patterns, the HSS is stable and coexists with the pattern allowing the formation of a LS. When a cell is lost the freed space is occupied by the HSS leading to a transient state formed by groups of LSs separated by the HSS, known as the cracking pattern [35]. If LSs have oscillatory tails they may lock at specific distances given by multiples of the oscillatory tail wavelength [36], thus, the cracking pattern is stationary. In microresonator nonlinear optics, stationary cracking patterns are also known as *soliton crystals* (SCs) [37–40]. In this context, cracking patterns formed by equally separated LSs are known as *superstructures* [37] or *perfect SCs* [40], whereas those with a random locking between LSs are named disordered SCs. On the contrary, if LS tails are monotonous, LSs repel each other, and the cracking pattern evolves towards a periodic solution with equally spaced peaks and a stable wave number (i.e., a perfect SC). In practice, a similar behavior is observed if tails are oscillatory with a wavelength much larger than the typical separation between peaks. This transient behavior can be extremely slow as the interaction decays exponentially with the distance [41,42] between peaks allowing for long-lived cracking patterns likely to be observed at second and even minute timescales in experiments.

In our numerical simulations [43], the Eckhaus instability is triggered by slowly ramping up the detuning and the pump parameter. This procedure is consistent with experimental

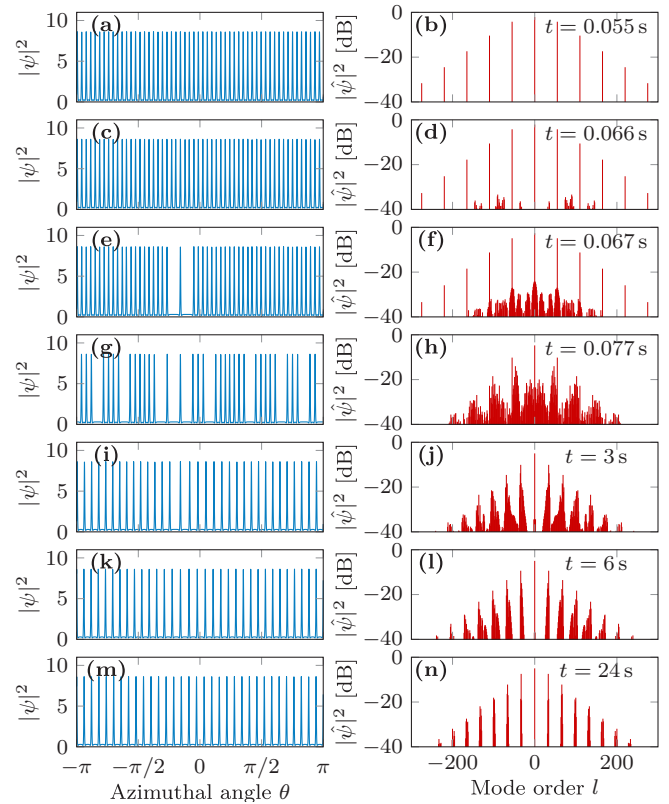


FIG. 3. Nonlinear evolution of the Eckhaus instability of the $L = 55$ (55 peaks) stripe pattern leading to the cracking of the pattern and, subsequent, convergence to a pattern with a lower stable wave-number $L = 33$ (33 peaks). The left column shows the spatial profile $|\psi(\theta)|^2$ of the pattern at different times, whereas the right column shows the corresponding power spectra $|\hat{\psi}(l)|^2$. Time stamps are given in real time $t = 2\tau_{\text{ph}} \times \tau = 10^{-6}\tau$. This numerical simulation shows that after the Eckhaus bifurcation the stripe pattern cracks, reducing the number of peaks from the initial 55 to 51 in panel (e), 35 in panel (g), and 33 in panel (i) to then very slowly converge towards a final perfectly periodic pattern with 33 peaks in a timescale of minutes. The time needed to simulate this 24 s-long transient dynamics was about 1 month, using a pseudospectral algorithm [43]. A movie of the simulation is available in the Supplemental Material [45].

systems where the detuning is thermally driven across the resonance [44]. The dashed line in Fig. 1 shows the ramp of parameter values used in the simulation shown in Fig. 3. A movie of the time evolution is also available in the Supplemental Material [45].

The simulation starts at $t = 0$ from a homogeneous initial condition with small random noise and with $\alpha = 1$ and $F = 1.05$, just above the MI. A stable pattern with $L = 55$ rapidly emerges, corresponding to the wave number with maximum growth rate L_u . The parameters are ramped up until $\alpha = 3.8$ and $F = 2$ at $t = 0.05$ s. These values are above the Eckhaus instability (Fig. 1). The simulation then continues up to $t = 24$ s (which corresponds to 24×10^6 photon lifetimes in our resonator) with clamped values for θ and F . The original pattern, whose spatial profile and power spectrum is shown Figs. 3(a) and 3(b), remains stable through the ramp until it crosses the EC line. At this point the pattern

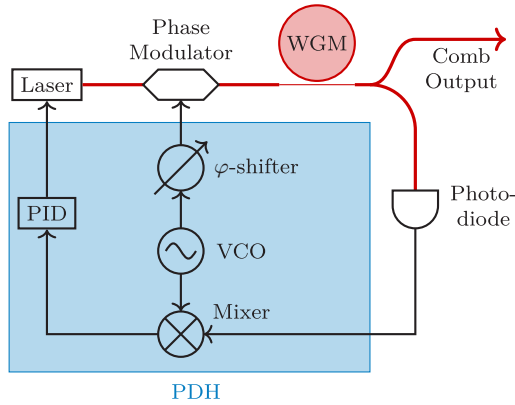


FIG. 4. Experimental setup. PID: Proportional-integral-derivative controller; VCO: voltage-controlled oscillator; PDH: Pound-Drever-Hall locking scheme; WGM: whispering-gallery mode resonator.

becomes unstable, and perturbations start to grow [Figs. 3(c) and 3(d)]. For the final ramp parameters the modes with fastest growth rate are located at half the Brillouin zone (Fig. 2). As a consequence some pattern cells disappear as shown in Figs. 3(e) and 3(f). Further development of the instability leads to a cracking pattern as shown in Figs. 3(g) and 3(h) for time $t = 0.077$ s. In analogy with solid-state crystals, these vacancies in the pattern are also known as Schottky defects [37]. For the parameters considered, LSs have oscillatory tails although the wavelength of the tail oscillations is much larger than the separation between consecutive peaks [46]. As a consequence, LSs do not get pinned, but they repel each other instead. This ultraslow dynamics can take times on the order of minutes to converge asymptotically to another pattern with a lower stable wave-number ($L = 33$ in this case) as shown in Figs. 3(i)–3(m). In contrast, in all nonlinear effects reported so far using the LLE, the transient dynamics usually last only a few τ_{ph} 's (i.e., a few microseconds in our case). The change in wave number from (a) to (m) is accompanied by a change in the envelope of the power spectra as the amplitudes of the fundamental Fourier component and its higher-order harmonics in a periodic solution depend on the wave number of the pattern. In this case the envelope becomes narrower indicating wider peaks in the final state. Note that if the ramp is increased to much larger values of the detuning, one reaches the single-soliton regime described in Ref. [47] and eventually only a single peak survives.

Such ultraslow dynamics are compatible with experimental observations in a MgF_2 WGM resonator. Our experimental system is displayed in Fig. 4. The resonator has an intrinsic quality factor $Q_{\text{in}} = 1.8 \times 10^9$ and is pumped by a resonant laser at 1552 nm. The resonator has a diameter of $d \simeq 11.8$ mm and a group-velocity refraction index of $n_g = 1.37$, yielding a FSR = $c/n_g\pi d \simeq 5.9$ GHz, where c is the velocity of light in vacuum. Further details on the experimental setup are given in Appendices A and B. When the resonator is pumped above threshold, stripe patterns emerging from a Turing or modulational instability can be excited inside the cavity. They are characterized by an integer number L of azimuthal rolls fitting the inner periphery of the disk.

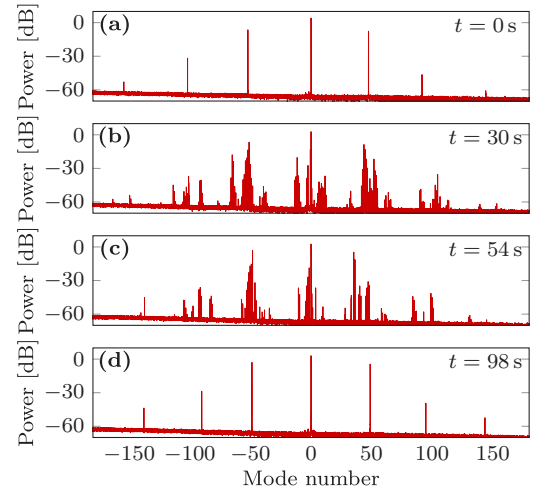


FIG. 5. Experimental evidence of ultraslow Eckhaus instability around a stripe pattern of wave-number $L = 50$ (a). The pattern becomes Eckhaus unstable with a temporal evolution characterized by minute timescale transients (b-c) before converging towards another pattern of lower-order with $L = 47$ (d).

Figure 5 shows an experimental example of the primary comb corresponding to a high-wave-number stripe pattern with $L = 50$. When the laser frequency is thermally driven across from the resonance, we observe the emergence of spurious peaks around the main primary comb, and the comb dynamics is characterized by a very slow timescale, that can be larger than a minute. This timescale appears *a priori* as inconsistent with the intrinsic Kerr comb dynamics where the slowest timescale is generally the photon lifetime $\tau_{\text{ph}} = Q/\omega_0 \sim 1 \mu\text{s}$ with $Q \sim 10^9$ being the loaded quality factor of our resonator, and ω_0 is the angular frequency of the pumped mode [48–50]. However, as shown earlier, this ultraslow timescale dynamics and the growth of spurious peaks around the main primary comb are compatible with an Eckhaus instability leading to very-long-lasting transient cracking patterns, and later on to a lower-order stable stripe pattern.

In conclusion, we have shown theoretically how the Eckhaus instability of a periodic pattern (primary comb) in whispering-gallery mode resonators can lead, for large detunings where the pattern is subcritical, to the cracking of the pattern and, subsequent, rearrangement of the remaining peaks in timescales six to eight orders of magnitude larger than the intracavity photon lifetime, which is the natural timescale for Kerr comb dynamics. This emerging timescale is dominated by the interaction between LSs. Despite the fact that we cannot completely overrule other possible mechanisms at play, the dynamics observed experimentally in a MgF_2 WGM resonator are compatible with the theoretical framework proposed in this paper. These results permit achieving a deeper understanding of secondary bifurcations in dissipative optical systems, and provide a theoretical framework to understand the formation of soliton crystals. Future work will investigate in detail the wide variety of spatiotemporal patterns that can be excited via these bifurcations, including when coinduced by other bulk nonlinearities [4,51,52].

ACKNOWLEDGMENTS

D.G. and Y.K.C. acknowledge support from Project ND-PHOT jointly funded by CSIC and CNRS. D.G. and P.C. acknowledge financial support from Agencia Estatal de Investigación (AEI, Spain) and Fondo Europeo de Desarrollo Regional under Project ESoTECoS, Grant No. FIS2015-63628-C2-1-R (AEI/FEDER,UE) and Agencia Estatal de Investigación through the María de Maeztu Program for Units of Excellence in R&D (Grant No. MDM-2017-0711). Y.K.C. also acknowledges funding from the European Research Council through the Projects NextPhase and Versyt from the *Centre National d'Etudes Spatiales* (CNES) through Project SHYRO. PPR acknowledges funding from the H2020 Marie Skłodowska-Curie Actions through the Project NOS-TER (101023717).

APPENDIX A: PROPERTIES, POLISHING PROCESS, AND CHARACTERIZATION OF THE WHISPERING-GALLERY MODE RESONATOR

Magnesium fluoride (MgF_2) is a tetragonal birefringent crystal with a transparency window ranging from UV to the midinfrared window (0.1–8 μm). It is used as material for the fabrication of lenses and polarizers. It has also been widely used for Kerr comb experiments at the telecom wavelength. Its transparency at 1550 nm makes it suitable for the fabrication of millimetric ultra-high- Q whispering-gallery mode resonators at the mentioned wavelength. Its refractive index is 1.3717 at 1550 nm and makes it suitable for taper coupling. From a commercially available crystalline MgF_2 WGM disk, consecutive steps of grinding and polishing allows us to achieve a quality factor of $\sim 10^9$, using an air-bearing spindle motor to spin the disk. During the grinding step, we used decreasing abrasive-coated size support to shape the resonator rim into a sharp “V” where the whispering-gallery mode will propagate. The second step consists of fine-grain polishing of the resonator via decreasing size abrasive particles down to 100 nm. Once the final polishing step is performed (surface roughness below 5 nm), we proceed to the characterization of the resonator in order to obtain its intrinsic, extrinsic, and loaded quality factor.

We have used the cavity-ring-down measurement technique to characterize the resonator quality factor. It is an efficient technique that allows avoiding thermal effects but permits, nevertheless, to obtain intrinsic, extrinsic, and loaded quality factors. A continuous-wave laser with a subkilohertz linewidth swept at a scanning speed of 1.2 GHz/ms is used to couple light into the resonator through the evanescent field of a tapered silica fiber. The recorded transmission is the temporal interference pattern between the laser input and the decaying resonance light. As shown in Fig. 6, a fitting of the experimental data gives an intrinsic quality factor of 1.82×10^9 , an extrinsic quality factor of 4.33×10^9 , and a loaded quality factor of 1.28×10^9 .

APPENDIX B: POUND-DREVER-HALL STABILIZATION SYSTEM

The PDH technique is designed to stabilize the pump laser wavelength to a particular resonance. It was initially used to

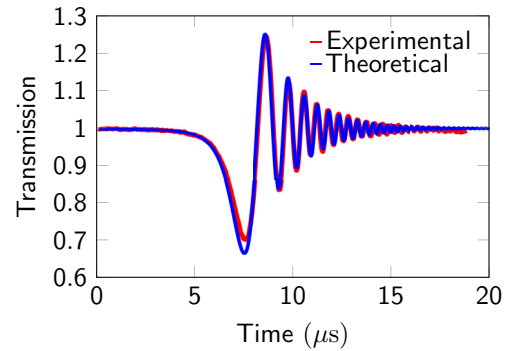


FIG. 6. Ring-down transmission spectrum. A theoretical fit gives an intrinsic quality factor of 1.82×10^9 , an extrinsic quality factor of 4.33×10^9 , and a loaded quality factor of 1.28×10^9 .

improve laser frequency stability by locking it on the mode of a cavity (more stable than the laser itself), thus, transferring the stability of the cavity mode frequency to the laser. It also has the effect of improving the linewidth of the locked laser if the mode linewidth is narrower than that of the laser. It has found many applications in very different fields, from the detection of gravitational waves to high-resolution spectroscopy. In our case, the PDH-locking technique is not used to improve the stability of the laser but rather to actively lock the laser onto an thermally unstable resonance of the whispering-gallery mode resonator.

WGM resonators are extremely sensitive to temperature and when light is injected inside a resonance, a part of the optical power is absorbed, causing the resonator to heat up. This effect both changes the refractive index and increases the diameter of the resonator via thermal dilatation, causing the resonances to shift. In order to control these effects, we actively lock the laser onto the resonance so that the laser follows the resonance as it shifts. We use a Toptica PDH module which generates the error signal, handles all communications with a computer, and drives the high-voltage source (0–150 V) needed to control the piezoelectric element in the external cavity of our laser (NKT adjustik).

The experimental setup is represented in Fig. 7. It features a narrow-linewidth (< 1 -kHz) continuous-wave laser operating around 1550 nm, which can be swept over 15 pm by applying a voltage on the piezoelectric element of the external cavity of the laser. A phase modulator is used in conjunction with the Toptica PDH module to phase modulate the laser and obtain an error signal. The laser then goes through a 90/10 optical coupler with 10% of the power being sent to a powermeter to have an image of the input power in the resonator, whereas the remaining 90% is sent in a polarization controller (PC) and then through a tapered fiber.

A WGM is coupled to the fiber, by sweeping the laser. We can observe the different coupled modes inside the resonator, and the polarization controller allows us to optimize the coupling of those modes. The WGM optical resonator that was used for this experiment is a 12-mm diameter MgF_2 disk, which was mechanically shaped and polished from a commercially available preform as explained in the preceding Appendix. The output of the resonator is then split into two paths, one leading the photodiode and the PDH module and

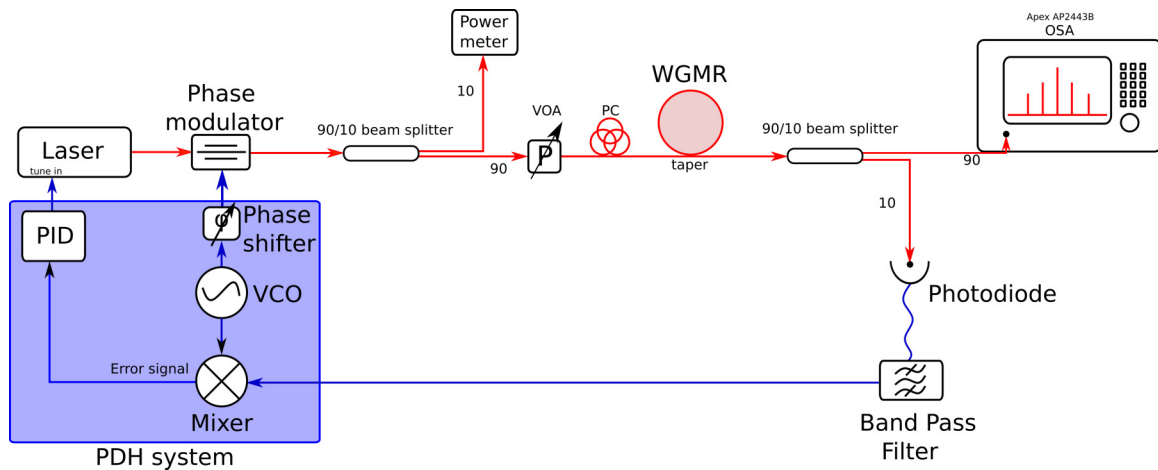


FIG. 7. Experimental setup used to generate frequency combs with a whispering-gallery mode resonator. Blue lines represent electrical paths, whereas, red lines represent optical paths.

the other path leading to a high-resolution optical spectrum analyzer (Apex AP2443B).

The experimental procedure is the following. The laser is scanned on the largest span possible. Depending on the coupling we will observe a certain number of modes. Among

those modes, we select the ones with a high coupling and high quality factor. The span is then reduced in order to sweep over only one mode. When Kerr comb generation is confirmed by the optical spectrum analyzer (OSA), the laser is then locked to that mode with the PDH module.

- [1] P. Del’Haye, A. Schliesser, O. Arcizet, T. Wilken, R. Holzwarth, and T. J. Kippenberg, Optical frequency comb generation from a monolithic microresonator, *Nature (London)* **450**, 1214 (2007).
- [2] T. J. Kippenberg, R. Holzwarth, and S. A. Diddams, Microresonator-based optical frequency combs, *Science* **332**, 555 (2011).
- [3] Y. K. Chembo, Kerr optical frequency combs: theory, applications and perspectives, *Nanophotonics* **5**, 214 (2016).
- [4] G. Lin, A. Coillet and Y. K. Chembo, Nonlinear photonics with high-Q whispering-gallery-mode resonators, *Adv. Opt. Photonics* **9**, 828 (2017).
- [5] A. Pasquazi, M. Peccianti, L. Razzari, D. J. Moss, S. Coen, M. Erkintalo, Y. K. Chembo, T. Hansson, S. Wabnitz, P. Del’Haye, X. Xue, A. M. Weiner, and R. Morandotti, Micro-combs: A novel generation of optical sources, *Phys. Rep.* **729**, 1 (2018).
- [6] C. Godey, I. V. Balakireva, A. Coillet and Y. K. Chembo, Stability analysis of the spatiotemporal Lugiato-Lefever model for Kerr optical frequency combs in the anomalous and normal dispersion regimes, *Phys. Rev. A* **89**, 063814 (2014).
- [7] P. Parra-Rivas, D. Gomila, M. A. Matias, S. Coen, and L. Gelens, Dynamics of localized and patterned structures in the Lugiato-Lefever equation determine the stability and shape of optical frequency combs, *Phys. Rev. A* **89**, 043813 (2014).
- [8] P. Parra-Rivas, E. Knobloch, D. Gomila and L. Gelens, Dark solitons in the Lugiato-Lefever equation with normal dispersion, *Phys. Rev. A* **93**, 063839 (2016).
- [9] C. Godey, A bifurcation analysis for the Lugiato-Lefever equation, *Eur. Phys. J. D* **71**, 131 (2017).
- [10] L. Delcey and M. Haragus, Periodic waves of the Lugiato-Lefever equation at the onset of Turing instability, *Philos. Trans. R. Soc. London A* **376**, 20170188 (2018).
- [11] F. Leo, L. Gelens, P. Emplit, M. Haelterman, and S. Coen, Dynamics of one-dimensional kerr cavity solitons, *Opt. Express* **21**, 9180 (2013).
- [12] P. Parra-Rivas, D. Gomila, L. Gelens, and E. Knobloch, Bifurcation structure of localized states in the Lugiato-Lefever equation with anomalous dispersion, *Phys. Rev. E* **97**, 042204 (2018).
- [13] P. Parra-Rivas, D. Gomila, L. Gelens, and E. Knobloch, Bifurcation structure of periodic patterns in the Lugiato-Lefever equation with anomalous dispersion, *Phys. Rev. E* **98**, 042212 (2018).
- [14] N. Périnet, N. Verschueren, and S. Coulibaly, Eckhaus instability in the Lugiato-Lefever model, *Eur. Phys. J. D* **71**, 243 (2017).
- [15] Z. Liu, F. Leo, S. Coulibaly, and M. Taki, Secondary instabilities in all fiber ring cavities, *Phys. Rev. A* **90**, 033837 (2014).
- [16] S. Coulibaly, M. Taki, A. Bendahmane, G. Millot, B. Kibler, and M. G. Clerc, Turbulence-Induced Rogue Waves in Kerr Resonators, *Phys. Rev. X* **9**, 011054 (2019).
- [17] W. Eckhaus, *Studies in Nonlinear Stability Theory* (Springer, New York, 1965).
- [18] D. Walgraef, *Spatio-Temporal Pattern Formation* (Springer, New York, 1997).
- [19] M. Cross and H. Greenside, *Pattern Formation and Dynamics in Nonequilibrium Systems* (Cambridge University Press, Cambridge, UK, 2009).
- [20] L. S. Tuckerman and D. Barkley, Bifurcation analysis of the Eckhaus instability, *Physica D* **46**, 57 (1990).
- [21] G. Ahlers, D. S. Cannell, M. A. Dominguez-Lerma, and R. Heinrichs, Wavenumber selection and Eckhaus instability in Couette-Taylor flow, *Physica D* **23**, 202 (1986).
- [22] M. Lowe and J. P. Gollub, Pattern Selection near the Onset of Convection: The Eckhaus Instability, *Phys. Rev. Lett.* **55**, 2575 (1985).

- [23] E. Louvergneaux, Pattern-Dislocation-Type Dynamical Instability in 1D Optical Feedback Kerr Media with Gaussian Transverse Pumping, *Phys. Rev. Lett.* **87**, 244501 (2001).
- [24] J. Plumecoq, C. Szewaj, D. Derozier, M. Lefranc, and S. Bielawski, Eckhaus instability induced by nonuniformities in a laser, *Phys. Rev. A* **64**, 061801(R) (2001).
- [25] F. Li, D. Huang, K. Nakkeeran, J. Nathan Kutz, J. Yuan, and P. K. A. Wai, Eckhaus instability in laser cavities with harmonically swept filters, *J. Lightwave Technol.* **39**, 6531 (2021).
- [26] M. Wolfrum and S. Yanchuk, Eckhaus Instability in Systems with Large Delay, *Phys. Rev. Lett.* **96**, 220201 (2006).
- [27] H. Riecke and H. G. Paap, Perfect Wave-Number Selection and Drifting Patterns in Ramped Taylor Vortex Flow, *Phys. Rev. Lett.* **59**, 2570 (1987).
- [28] G. Lin and Y. K. Chembo, On the dispersion management of fluorite whispering-gallery mode resonators for Kerr optical frequency comb generation in the telecom and mid-infrared range, *Opt. Express* **23**, 1594 (2015).
- [29] L. A. Lugiato and R. Lefever, Spatial Dissipative Structures in Passive Optical Systems, *Phys. Rev. Lett.* **58**, 2209 (1987).
- [30] A. B. Matsko, A. A. Savchenkov, W. Liang, V. S. Ilchenko, D. Seidel, and L. Maleki, Mode-locked Kerr frequency combs, *Opt. Lett.* **36**, 2845 (2011).
- [31] Y. K. Chembo and C. R. Menyuk, Spatiotemporal Lugiato-Lefever formalism for Kerr-comb generation in whispering-gallery-mode resonators, *Phys. Rev. A* **87**, 053852 (2013).
- [32] S. Coen, H. G. Randle, T. Sylvestre, and M. Erkintalo, Modeling of octave-spanning Kerr frequency combs using a generalized mean-field Lugiato-Lefever model, *Opt. Lett.* **38**, 37 (2013).
- [33] K. Saleh and Y. K. Chembo, On the phase noise performance of microwave and millimeter-wave signals generated with versatile Kerr optical frequency combs, *Opt. Express* **24**, 25043 (2016).
- [34] D. Gomila and P. Colet, Dynamics of hexagonal patterns in a self-focusing Kerr cavity, *Phys. Rev. E* **76**, 016217 (2007).
- [35] G. K. Harkness, W. J. Firth, G.-L. Oppo, and J. M. McSloy, Computationally determined existence and stability of transverse structures. I. Periodic optical patterns, *Phys. Rev. E* **66**, 046605 (2002).
- [36] P. Parra-Rivas, D. Gomila, P. Colet, and L. Gelens, Interaction of solitons and the formation of bound states in the generalized Lugiato-Lefever equation, *Eur. Phys. J. D* **71**, 198 (2017).
- [37] D. C. Cole, E. S. Lamb, P. DelHaye, S. A. Diddams, and S. B. Papp, Soliton crystals in Kerr resonators, *Nat. Photonics* **11**, 671 (2017).
- [38] H. Taheri, A. B. Matsko, and L. Maleki, Optical lattice trap for Kerr solitons, *Eur. Phys. J. D* **71**, 153 (2017).
- [39] W. Wang, Z. Lu, W. Zhang, S. T. Chu, B. E. Little, L. Wang, X. Xie, M. Liu, Q. Yang, L. Wang, J. Zhao, G. Wang, Q. Sun, Y. Liu, Y. Wang, and W. Zhao, Robust soliton crystals in a thermally controlled microresonator, *Opt. Lett.* **43**, 2002 (2018).
- [40] M. Karpov, M. H. Pfeiffer, H. Guo, W. Weng, J. Liu, and T. Kippenberg, Dynamics of soliton crystals in optical microresonators, *Nat. Phys.* **15**, 1071-1077 (2019).
- [41] P. Couillet, C. Elphick, and D. Repaux, Nature of Spatial Chaos, *Phys. Rev. Lett.* **58**, 431 (1987).
- [42] P. Couillet, Localized patterns and fronts in nonequilibrium systems, *Int. J. Bifurcation Chaos Appl. Sci. Eng.* **12**, 2445 (2002).
- [43] Numerical simulations of the Lugiato-Lefever equation are performed using a pseudospectral method where the linear terms in Fourier space are integrated exactly whereas the nonlinear ones are integrated using a second-order approximation in time. A 1D lattice of 4096 points was used. The time t in seconds is expressed as $t = 10^{-6}\tau$, where τ is the dimensionless time of the LLE. The time step for numerical integration was $\Delta\tau = 0.001$.
- [44] S. Diallo, G. Lin, and Y. K. Chembo, Giant thermo-optical relaxation oscillations in millimeter-size whispering gallery mode disk resonators, *Opt. Lett.* **40**, 3834 (2015).
- [45] See Supplemental Material at <http://link.aps.org/supplemental/10.1103/PhysRevA.106.053518> for a movie of the time evolution shown in Fig. 3. The upper panel shows the intracavity field in the rotating frame whereas the bottom panel shows its corresponding frequency comb (Fourier transform). The time τ and the current value of the detuning are displayed in the top right corner of the bottom panel.
- [46] The wavelength of the spatial oscillations in the tails of the LS calculated from the imaginary part of the spatial eigenvalues of the HSS [36] for the parameters used in the simulations is $\pi/6.59$, larger than the typical separation between peaks.
- [47] T. Herr, V. Brasch, J. D. Jost, C. Y. Wang, N. M. Kondratiev, M. L. Gorodetsky, and T. J. Kippenberg, Temporal solitons in optical microresonators, *Nat. Photonics* **8**, 145 (2014).
- [48] Y. K. Chembo and N. Yu, On the generation of octave-spanning optical frequency combs using monolithic whispering-gallery-mode microresonators, *Opt. Lett.* **35**, 2696 (2010).
- [49] A. Coillet, R. Henriot, K.-P. Huy, M. Jacquot, L. Furfaro, I. Balakireva, L. Larger, and Y. K. Chembo, Microwave photonics systems based on whispering-gallery-mode resonators, *J. Vis. Exp.* **78**, e50423 (2013).
- [50] R. Henriot, G. Lin, A. Coillet, M. Jacquot, L. Furfaro, L. Larger and Y. K. Chembo, Kerr optical frequency comb generation in strontium fluoride whispering-gallery mode resonators with billion quality factor, *Opt. Lett.* **40**, 1567 (2015).
- [51] G. Lin and Y. K. Chembo, Phase-locking transition in Raman combs generated with whispering gallery mode resonators, *Opt. Lett.* **41**, 3718 (2016).
- [52] G. Lin, S. Diallo, J. M. Dudley and Y. K. Chembo, Universal nonlinear scattering in ultra-high Q whispering-gallery mode resonators, *Opt. Express* **24**, 14880 (2016).